Japanese Journal of Applied Physics **53**, 07KC03 (2014) **REGULAR PAPER**
http://dx.doi.org/10.7567/JJAP.53.07KC03

Feasibility of low-frequency directive sound source with high range resolution using pulse compression technique

Hideyuki Noumura*, Hideo Adachi, Tomoo Kamakura, and Gregory T. Clement†

The University of Electro-Communications, Chofu, Tokyo 182-8585, Japan
E-mail: h.nomura@uec.ac.jp

Received November 28, 2013; accepted March 24, 2014; published online June 12, 2014

The lateral resolution of a parametric acoustic array with narrow directivity is expected to be superior to that of a conventional linear sound source. The range resolution of the parametric array, however, is as low as the resolution of the linear source because of its long wavelength. To improve the range resolution in maintaining a high azimuth resolution for parametric sounds, a pulse compression technique using linear frequency-modulated signals or chirp signals is explored in the present study. The generation of chirp-modulated parametric sounds was experimentally confirmed in water, and then the auto-correlation of the parametric sound demonstrates short pulse widths up to 1/10 of the primary pulse duration. The results reveal that the pulse compression is feasible for a low-frequency parametric sound source with narrow directivity in the same manner as the compression of a linear sound wave.

1. Introduction

Increasing the radiation frequency of a sound source with a finite aperture narrows its directivity and shortens the wavelength, i.e., lateral as well as range resolutions are improved generally in nondestructive tests and ultrasound imaging devices in ultrasonic measurements and medical instruments.[1–3] For example, commercially available ultrasound imaging devices, e.g., ultrasonography in medicine, typically operate at a frequency greater than 2.5 MHz and the corresponding wavelength that basically determines the range resolution is less than 0.6 mm. Since ultrasound at high frequencies is, however, much attenuated by medium viscosity, the penetration depth is limited. Hence, applications of high-frequency ultrasound to measurement and imaging in high attenuation media, e.g., oil, muddy water, the human body with fat and so on, have been confined to a relatively shallow region from the surface. In addition, a directive ultrasound source generates sidelobes and repetitions of peaks and dips in the near field owing to diffraction. These involved sound fields therefore induce artifacts in imaging, so that images are degraded in quality. These disadvantages make it difficult to apply ultrasound at high frequency in a wide range from the near- to far-field of a sound source to ultrasound measurement and imaging. A directive sound source at low frequency with no sidelobes such as a parametric source[4–9] is a possible solution to resolve these problems.

Incidentally, parametric sources have been applied, for example, as a sub-bottom profiler system that can visualize layered configurations below the seabed.[10] The disadvantages of a parametric source on measurement and imaging are a low range resolution owing to its long wavelength and a low signal level, i.e., a low signal-to-noise ratio (SNR) originating from a nonlinear phenomenon. To resolve such problems, a promising method is to apply a pulse compression technique to parametric sounds.

The pulse compression technique was originally developed in radar to detect distance compatible with spatial resolutions.[11,12] The basic concept of the pulse compression technique improves pulse width and SNR by modulating transmitting signals and by performing appropriate signal processing. This technique is also actively applied to ultrasonic imaging to improve SNR.[13–17] The pulse compression technique for nonlinear signals has also been performed so far. These nonlinear methods were performed by isolating higher harmonic components, which are then signal-processed in a similar manner to linear pulse compression.[18–20]

We have already proposed an alternative approach that is different from the nonlinear compression technique consisting of the fundamental and higher harmonics and have verified that effective compression in pulse width is realized even if we use a high Q transducer.[21] It is then expected that the pulse compression technique is applicable to parametric sound to improve range resolution.

The final goal of our study is to develop an acoustic imaging system using a low-frequency directive sound source with high spatial resolution in a wide range from the near- to far-field and to establish an acoustical visualization concept even in a high-attenuation medium. The present paper is organized as follows. First, we show the generation of a chip-modulated parametric sound for pulse compression. Then, we calculate the auto-correlation function (ACF) to compress the parametric sound. We finally quantitatively evaluate the compressed pulse widths from experimental and theoretical points of view.

2. Theory

When two finite-amplitude primary waves at different but neighboring frequencies are propagating in the same direction, sum and difference frequency sounds are generated along the primary waves owing to the nonlinearity of a medium. In particular, the parametric sound of the difference frequency forms a very narrow beam width almost the same as those of the primary waves, although its frequency is low.[4,5]

In this study, a pulse compression technique with linear frequency-modulated or chirp signals is applied to a parametric sound source to improve the low range resolution that is due to its long wavelength. Figure 1 shows a basic concept illustrating distance measurement or imaging systems using parametric sounds. The experimental procedure is described as follows:

†Present address: Department of Biomedical Engineering, Cleveland Clinic, Beachwood, OH 44122, U.S.A.

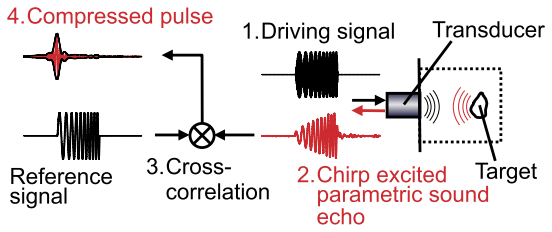

Fig. 1. (Color online) Pulse compression of parametric sound echo.

(1) Finite amplitude ultrasounds are radiated from a sound source driven by a modulated signal that generates chirp-modulated parametric sounds.
(2) Chirp-modulated parametric sounds are generated during propagation owing to the nonlinearity of water, and reflection echo signals of the parametric sounds from a target are received by a receiving transducer.
(3) A cross-correlation function (CCF) between the echo and reference signals is computed.
(4) Finally, the cross-correlation indicates the distance between the source and target. Images are obtained by scanning the sound source mechanically or electrically.

In this study, a transmitting transducer is driven by the sum signal of $s_1(t) + s_2(t)$ to generate chirp-modulated parametric sound;

$$s_1(t) = \begin{cases} A_1 \sin\left(2\pi\left\{f_0 + \frac{f_{\text{start}}}{2}\right\}t + \frac{1}{4}\mu t^2\right) & \text{for } 0 \le t \le T_s, \\ 0 & \text{otherwise,} \end{cases} \quad (1)$$

$$s_2(t) = \begin{cases} A_2 \sin\left(2\pi\left\{f_0 - \frac{f_{\text{start}}}{2}\right\}t - \frac{1}{4}\mu t^2\right) & \text{for } 0 \le t \le T_s, \\ 0 & \text{otherwise,} \end{cases} \quad (2)$$

where $s_1(t)$ is an up-chirp signal and $s_2(t)$ is a down-chirp signal. In this case, the parametric sound consists of a linear up-chirp signal. In Eqs. (1) and (2), t is time and f_0 is the center frequency of the driving signal. Furthermore, A_1 and A_2 are the amplitudes of chirp signals, $\mu = 2\pi B/T_s$ is the angular sweep ratio, $B = f_{\text{stop}} - f_{\text{start}}$ is the chirp bandwidth, f_{start} and f_{stop} are the start and stop frequencies of the chirp signal, respectively, and T_s is the sweep time. $f_1(t)$ and $f_2(t)$ in Fig. 2 are the instantaneous frequencies of the signals $s_1(t)$ and $s_2(t)$, respectively. The instantaneous difference frequency $f_d(t)$ is then given by

$$f_d(t) = f_{\text{start}} + \frac{\mu}{2\pi}t = f_{\text{start}} + \frac{B}{T_s}t \quad \text{for } 0 \le t \le T_s. \quad (3)$$

The operation of cross-correlation between echo and reference signals is generally performed for distance measurements and imaging. In the present study, however, an ACF is obtained in place of cross-correlation to evaluate the fundamental performance of pulse compression for chirp-modulated parametric sounds.

3. Experiment

3.1 Experimental setup

The feasibility of the pulse compression technique for parametric sound was experimentally evaluated, especially to obtain the compressed pulse width. First, the generation of chirp-modulated parametric sounds of 100 to 400 kHz bandwidth by the nonlinear interaction of primary ultrasounds was experimentally confirmed in water. The center frequency of primary frequency was 2.1 MHz. The pulse compression of parametric sounds received by a hydrophone was performed and the efficiency was evaluated. The experimental setup is shown in Fig. 3.

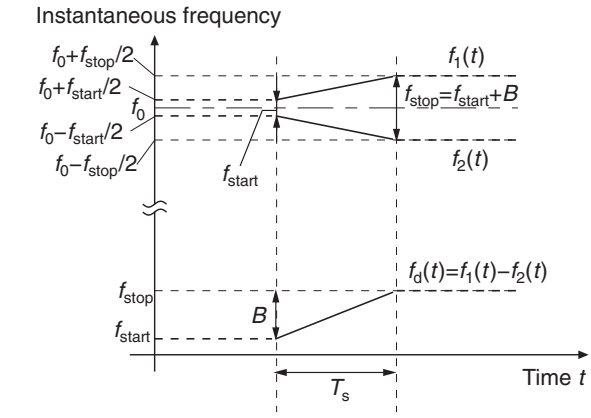

Fig. 2. Instantaneous frequencies of driving signals and difference frequency signal.

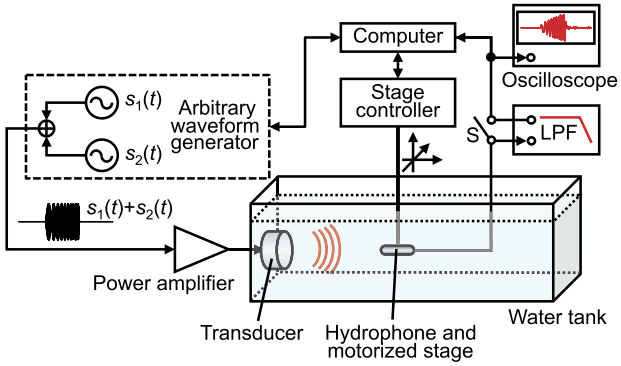

Fig. 3. (Color online) Experimental setup. The switch S is closed when receiving primary waves and opened when receiving parametric sounds.

A circular aperture ultrasonic transducer (Sonix IY0225) of 1 inch in diameter and 2.1 MHz in resonance frequency was used as a sound source in the experiment. The fractional bandwidth of the transducer is about 0.3. Primary ultrasounds at several MHz were received by a needle type hydrophone (Force Technology MH28-10) with almost uniform sensitivity in a MHz frequency range, and parametric sounds at several hundred kHz were received by another hydrophone (Reson TC4048) with a uniform frequency response below 500 kHz. Driving signals were generated by an arbitrary waveform generator (NF 1966) and amplified by a power amplifier (Kalmus 150C). When only parametric sounds were needed, a low pass filter (NF 36328) with a cut-off frequency of 700 kHz followed the preamplifier of the low-frequency hydrophone because the amplitude of the parametric sound is too small to precisely extract its spectral component from the received signals whose magnitudes are almost predominated by the primary ultrasounds. Received signals were sent through a digital oscilloscope (LeCroy 6051A) at an 8 bit vertical resolution, and the ACFs were calculated using a computer as post-processing.

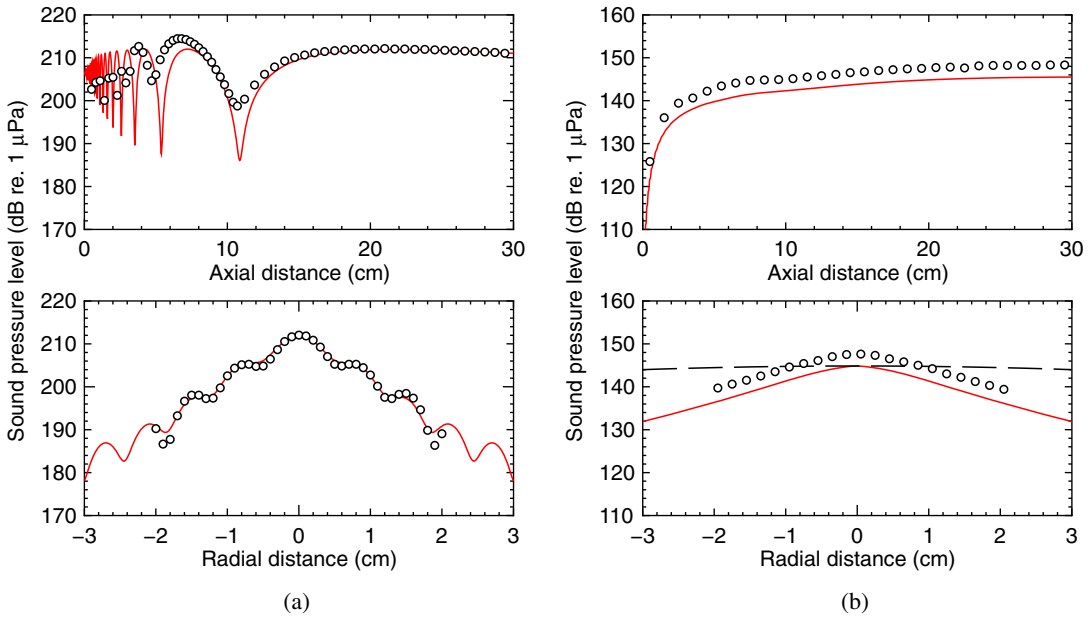

Fig. 4. (Color online) Pressure distributions of the primary sound at a center frequency of 2.1 MHz in (a) and of the parametric sound at a difference frequency of 100 kHz generated from the sound source driven by the sum of 2.05 and 2.15 MHz sinusoid signals in (b). The upper and lower figures show the axial pressure curves and radial beam patterns at 20 cm from the source, respectively. The symbols and solid curves indicate the measured and theoretical sound pressure amplitudes, respectively, and the dashed curve indicates the linear sound pressures of 100 kHz radiated from a sound source with the same aperture, whose pressure is adjusted to the same as that of the parametric sound on the beam axis.

The output voltage of the arbitrary waveform generator was determined so that the sound pressure amplitude on the transducer driven at 2.1 MHz was estimated to be about 30 kPa, and this voltage was kept constant during experiments. This meant that the amplitudes A_1 and A_2 in Eqs. (1) and (2) had same the values. However, the sound pressure amplitudes, which corresponded to A_1 and A_2, were relatively lower than 30 kPa, because of the frequency characteristic of the transducer with a center frequency of 2.1 MHz, and depended on the instantaneous frequency of the driving signal.

3.2 Sound field

Figure 4 shows the measurement data of the primary sound pressures generated from the sound source driven at a resonance frequency of 2.1 MHz in (a) and of the parametric sound pressures of 100 kHz when the source is driven at 2.05 and 2.15 MHz in (b). Sound pressure distributions along the beam axis and radial pressure patterns perpendicular to the beam axis at 20 cm from the source are plotted with theoretical predictions. The predictions are numerical simulations based on the governing equations of a compressible viscous fluid. The details of the simulation method have been described in a previous paper.[9)]

The experimental and theoretical data reveal that the parametric pressure curve has a smooth slope to 10 cm far away from the sound source. In contrast, the primary curve has peaks and dips in amplitude near the source, although a smooth slope is seen to 20 cm far away from the source.

The comparison between the primary and parametric sounds indicates that the level of the parametric sound is about 60 dB lower than that of the primary sound. However, since the parametric sound accumulatively increases with propagation distance even after primary sounds decrease by attenuation and spherical diffusion, the level difference decreases with distance. For example, in the case of ultrasonic propagation of at 2 MHz in soft tissue with an attenuation coefficient of 1 dB/(MHz·cm), the level coincides with the level of parametric sound at a propagation distance of 30 cm. In addition, the low SNR of parametric sound is improved by introducing a receiving element with high sensitivity at only several hundred kHz, which is the frequency range of parametric sound.[22)]

The radial pattern of 100 kHz linear sound radiated from the same aperture source is plotted in Fig. 4(b) for comparison with the parametric sound beam. This comparison clearly indicates that the parametric sound beam is narrower than the linear sound beam. From this result, the directivity and lateral resolution of the low-frequency sound source are improved by the introduction of the parametric sound source at difference frequency.

The measured pressure data of the primary wave agree well with the theory, although the pressure amplitude of the parametric sound is about 4 dB higher than the prediction. A possible source for such discrepancies is probably the hydrophone sensor element that responds nonlinearly to finite amplitude pressures of the primary waves. Another possible source is the accuracy in pressure calibration of the hydrophone. For example, an error of 2 dB in primary sound measurements causes an error of 4 dB in parametric sound measurements.

3.3 Chirp-modulated parametric sound

The center frequency f_0 and the start frequency f_{start} of chirp signals in Eqs. (1) and (2) were kept at 2.1 MHz and 100 kHz, respectively, except for varying the chirp bandwidth B from 100 to 400 kHz by 100 kHz steps. The corresponding sweep time was changed depending on the bandwidths under

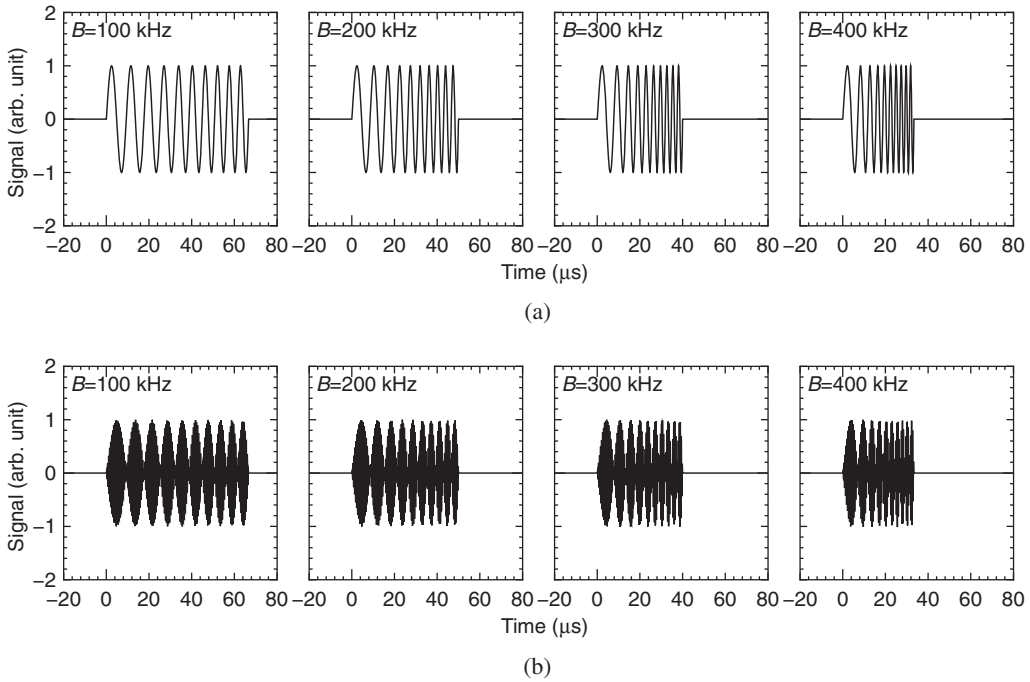

Fig. 5. Original signals: reference signals (a), which are desired parametric sounds, and modulated primary signals (b) to drive the transmitting transducer.

Table I. Sweep time for chirp-modulated parametric sounds of 10 cycles.

Bandwidth B (kHz)	Sweep time T_s (μs)
100	66.7
200	50.0
300	40.0
400	33.3

the generation of ten-cycle parametric sounds (see Table I). Figure 5 shows reference signals or desired chirp parametric signals, and modulated primary signals, which are described by the sum signals of Eqs. (1) and (2).

Figures 6(a) and 6(c) show on-axis primary and parametric waveforms experimentally observed at 20 cm from the sound source. Numerical simulations are also shown for comparison in Figs. 6(b) and 6(d) subject to the experimental source conditions. Both the received parametric signals in Figs. 6(c) and 6(d) indicate up-chirp signals similar to the reference signals in Fig. 5(a). It should be noted that differences in amplitude are clearly seen between the parametric sound and reference signals; i.e., the amplitudes of the reference signals are independent of time, while the parametric signals are increased with time.

The parametric sound at difference frequency is generated with a breakdown in the symmetry of positive and negative envelopes of amplitude modulated primary sound, and is originated with the waveform distortion or phase change of the primary sound. This phase change is limited by the period and amplitude of the primary sound, and increases with the increase in difference frequency.[23] This phenomenon is theoretically explained by that the decrease of the down-shift ratio, which is defined as the primary frequency f_0 to the difference frequency f_d, increases the pressure amplitude of parametric sound.[24] In the present study, the primary sound frequency and the start frequency of the chirp signal remain unchanged, and only the chirp bandwidth is changed. Therefore, broadening the chirp bandwidth, which corresponds to the decreases of the down shift ratio and increasing the stop frequency, increases the instantaneous amplitude of the parametric sound with time.

The experimental and simulated results of received ultrasounds are in good agreement, although the amplitude of the parametric sound obtained by experiment is 2 or 3 times larger than the simulation results. The primary reasons for this difference seem to be the nonlinear response of the hydrophone exposed to finite amplitude primary waves and calibration accuracy, as described in Sect. 3.1.

3.4 Pulse compression of parametric sound

To verify the application effects of the pulse compression technique to the improvement of range resolution for low-frequency parametric sounds, we calculated ACFs for parametric sounds. ACFs at 20 cm obtained by experiment and simulation are shown in Figs. 7(a) and 7(b), where the amplitudes of all the ACFs are normalized by the maximum value when the bandwidth B is 400 kHz. In the figure, the envelope functions of ACFs are plotted as dotted lines. As can be seen, the experimental results are in good agreement with the corresponding simulations on the whole. Additionally, the sweep times that are originally several ten μs are greatly compressed to short pulse widths of about several micro-seconds. It is also observed that increasing the chirp bandwidth tends to decrease the compressed pulse width.

The amplitude of ACF tends to increase with the chirp bandwidth. As indicated in Fig. 6, this tendency is due to the fact that the amplitude of the parametric sound with a wider chirp bandwidth is larger than that with a narrower bandwidth.

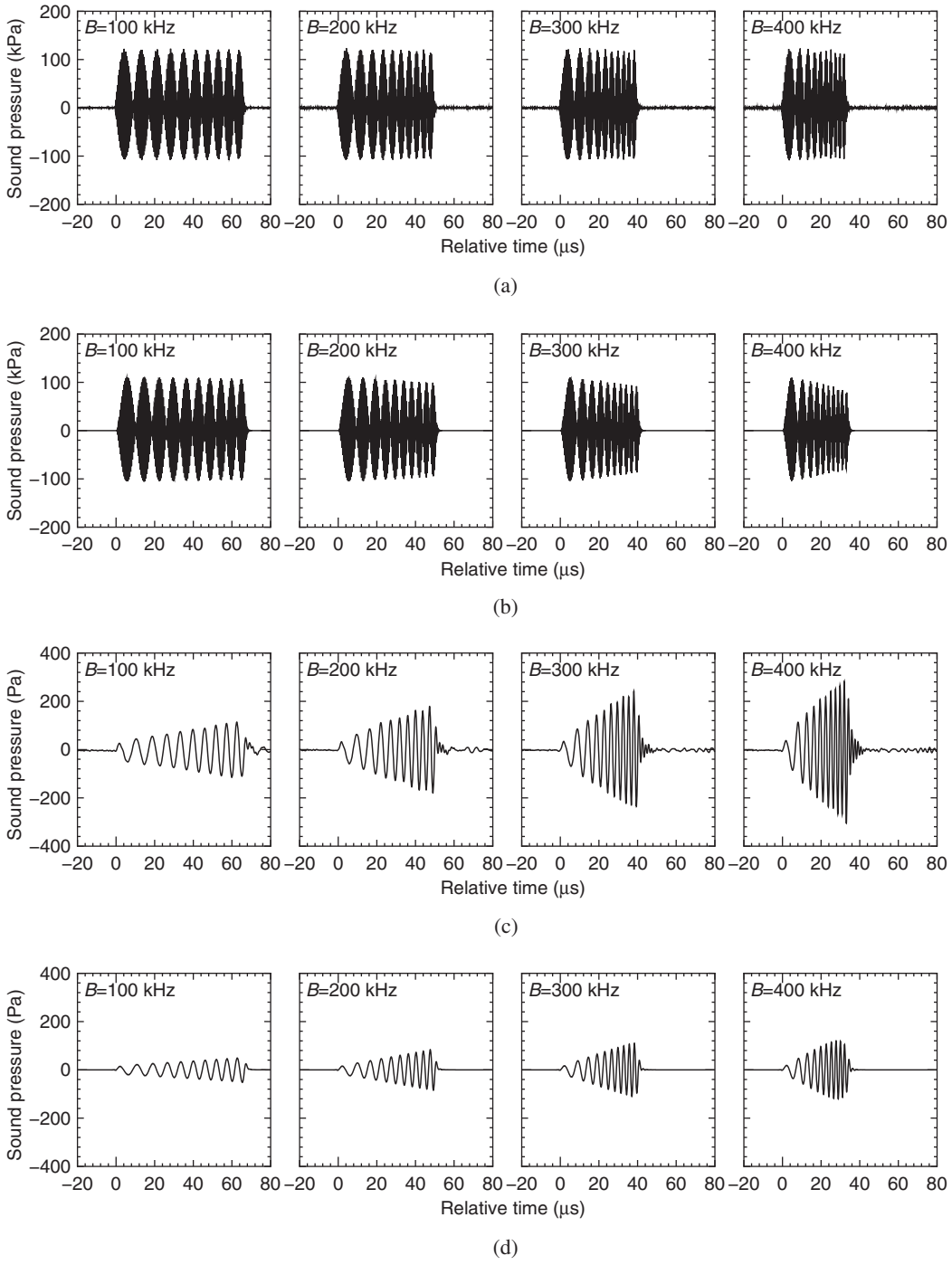

Fig. 6. Observed ultrasounds at 20 cm from the source. Waveforms (a) and (b) are the ultrasounds obtained by experiment and simulation, respectively. (c) and (d) are the corresponding chirp-modulated parametric sounds obtained by experiment and simulation, respectively.

To quantitatively evaluate the pulse compression of parametric sound, the compressed pulse width is estimated as a function of chirp bandwidth. The pulse widths obtained from the present experiment are plotted in Fig. 8(a) with the prediction that is theoretically in inverse proportion to the chirp bandwidth,[11,12] in which the pulse width is defined as -3 dB relative to the maximum amplitude of the ACF envelope. In addition, the compressed pulse width obtained from the simulation[25] and that optimally obtained from the ACF of the reference signal described in Fig. 5(a) are plotted together in Fig. 8(b). The pulse widths of the experiment and simulation are almost in good agreement. However, those are slight broader than that of the reference signal. This discrepancy suggests that there is a possibility to improve the compressed pulse width of parametric sound a little more.

The compressed pulse width at $B = 400$ kHz is 2.4 μs and is the narrowest among the pulses of four bandwidths. The range resolution, which is obtained by multiplying the pulse width by sound speed 1500 m/s, results in about 3.6 mm in water when B is 400 kHz. The duration of the primary (parametric) pulse in this case is 33.3 μs, corresponding to the range resolution of 49.6 mm. Hence, this comparison indicates that the range resolution is improved to more than

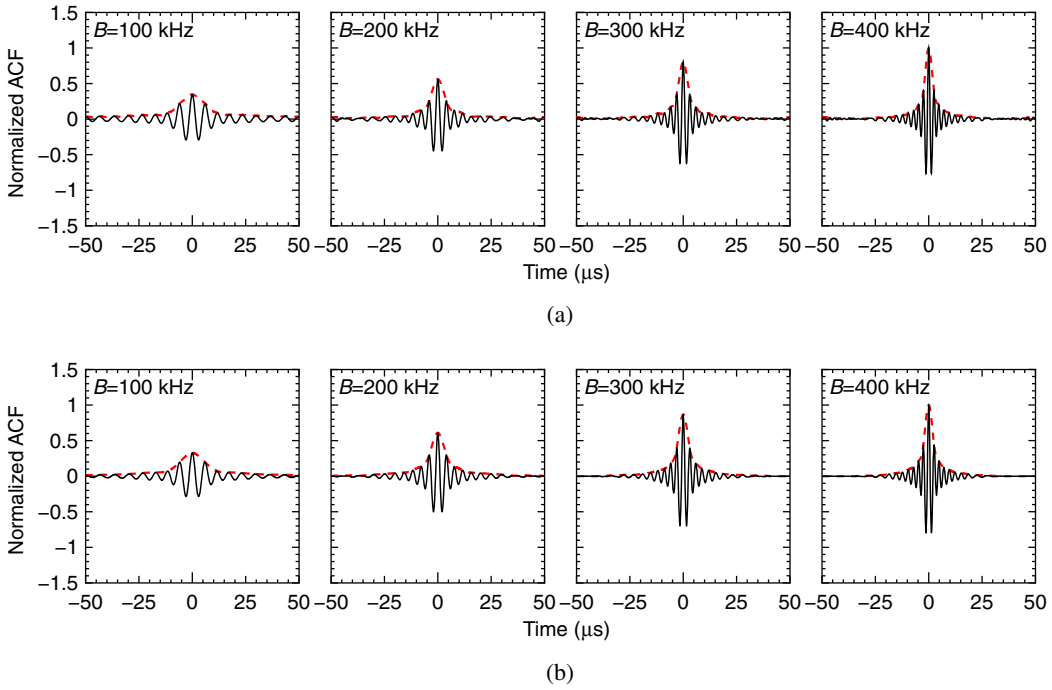

Fig. 7. (Color online) Pulse compression of parametric sounds observed at 20 cm from the sound source by experiment (a) and simulation (b). All the ACFs are normalized by the maximum value when B is 400 kHz. Solid and dotted curves indicate the ACFs and their envelope functions, respectively.

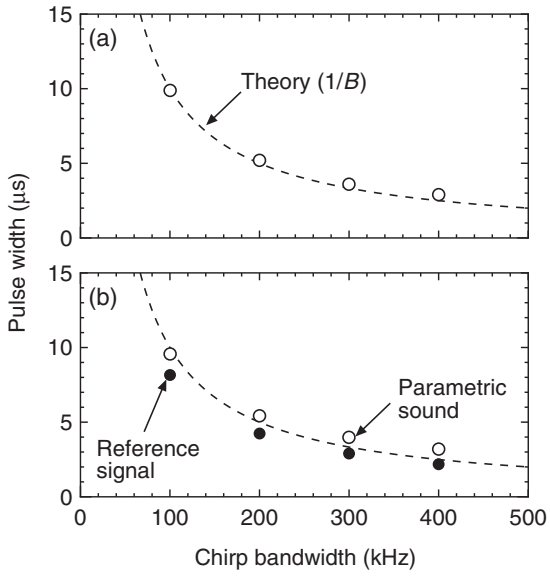

Fig. 8. Compressed pulse width of parametric sound observed at 20 cm from the sound source: (a) experiment and (b) simulation. For comparison, the pulse width of the ACF of the reference signal is plotted in (b). The pulse width is estimated at the width as −3 dB of the maximum amplitude of the envelope of ACF.

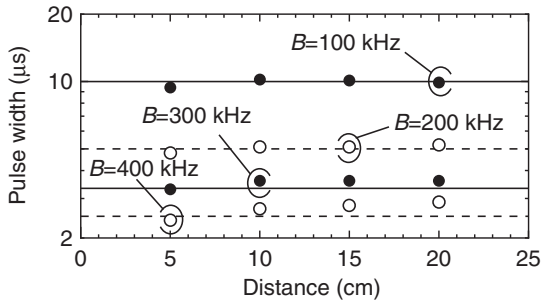

Fig. 9. Pulse width as a function of distance. Solids and curves indicate the experimental and theoretical values, respectively.

1/10 by the pulse compression. It then follows that the pulse compression technique is useful for realizing a low-frequency directive sound source with high range resolution.

Our concern is whether the compressed pulse width of the parametric sound depends on the distance from the source, since the pressure amplitude of the parametric sound accumulatively increases with propagation distance and the rate of the accumulation depends on the frequency,[5] as described in Fig. 4. Being different from the theory that exhibits distance-independence, the measured compressed pulse width of the parametric sound is slightly dependent on distance, as shown in Fig. 9.

The operation of cross-correlation between echo and reference signals is needed for distance measurements and imaging. This implies that the time dependence of chirp-modulated parametric sound amplitude affects the pulse compression. The CCF between the obtained signal and reference signal, as shown in Fig. 5(a), indicated that the pulse width of CCF was about 5% wider than that of ACF, and the maximum amplitude of CCF was about 20% larger than that of CCF. These results suggest that it is important to consider an optimal reference signal or the generation of chirp-modulated parametric sound with time-independent amplitude.

4. Conclusions

The improvement of range resolution for parametric sounds was challenged to realize a low-frequency directive sound source with high range resolution. The present studies

confirmed that the chirp-modulated parametric waveforms obtained in the experiment almost agree with the corresponding simulated waveforms except for their amplitudes. To evaluate the performance of pulse compression, the ACFs of the parametric sounds were calculated. The pulse width of the compressed parametric sound with a chirp width of 400 kHz was 2.4 μs, which corresponds to a range resolution of about 3.6 mm, although the duration time of received parametric sounds was long to be 33.3 μs. The result thus suggests that the pulse compression technique seems to be useful for parametric sound, and for the realization of a low-frequency directive sound source with high range resolution.

Since a parametric acoustic array is formed by nonlinear effects, the sound pressure, and thus SNR, is generally not high. For a practical situation, the estimation of parametric sound echoes from targets, effective receiving methods of the echoes, and evaluation of image quality obtained by the present pulse compression remain for examination as further studies.

Acknowledgments

This work was supported in part by JSPS Grants-in-Aid for Scientific Research (22760619 and 2535062) and the Regional Innovation Strategy Support Program, the Ministry of Education, Culture, Sports, Science and Technology, Japan.

1) M. Ikeuchi, K. Jinno, Y. Ohara, and K. Yamanaka, Jpn. J. Appl. Phys. **52**, 07HC08 (2013).
2) M. Fukuda and K. Imano, Jpn. J. Appl. Phys. **51**, 07GB06 (2012).
3) T. Yamamura, M. Tanabe, K. Okubo, and N. Tagawa, Jpn. J. Appl. Phys. **51**, 07GF01 (2012).
4) P. J. Westervelt, J. Acoust. Soc. Am. **35**, 535 (1963).
5) G. S. Garrett, J. N. Tjøtta, and S. Tjøtta, J. Acoust. Soc. Am. **74**, 1013 (1983).
6) K. Hashiba and H. Masuzawa, Jpn. J. Appl. Phys. **42**, 3227 (2003).
7) S. Saito, T. Tsubono, and N. Kamata, Jpn. J. Appl. Phys. **41**, 3159 (2002).
8) T. Kamakura, H. Nomura, M. Akiyama, and C. M. Hedberg, Acta Acust. United Acust. **97**, 209 (2011).
9) H. Nomura, C. M. Hedberg, and T. Kamakura, Appl. Acoust. **73**, 1231 (2012).
10) J. Wunderlich, G. Wendt, and S. Müller, Mar. Geophys. Res. **26**, 123 (2005).
11) J. R. Klauder, A. C. Price, S. Darlington, and W. J. Albersheim, Bell Syst. Tech. J. **39**, 745 (1960).
12) C. Cook and J. Paolillo, Proc. IEEE **52**, 377 (1964).
13) T. X. Misaridis, K. Gammelmark, C. H. Jørgensen, N. Lindberg, A. H. Thomsen, M. H. Pedersen, and J. A. Jensen, Ultrasonics **38**, 183 (2000).
14) M. H. Pedersen, T. X. Misaridis, and J. A. Jensen, Ultrasound Med. Biol. **29**, 895 (2003).
15) T. Misaridis and J. A. Jensen, IEEE Trans. Ultrason. Ferroelectr. Freq. Control **52**, 177 (2005).
16) M. Tanabe, T. Yamamura, K. Okubo, and N. Tagawa, Jpn. J. Appl. Phys. **49**, 07HF15 (2010).
17) R. Toh and S. Motooka, Jpn. J. Appl. Phys. **48**, 07GB09 (2009).
18) J. M. G. Borsboom, C. T. Chin, and N. de Jong, Ultrasound Med. Biol. **29**, 277 (2003).
19) Y. Sun, D. E. Kruse, and K. W. Ferrara, IEEE Trans. Ultrason. Ferroelectr. Freq. Control **54**, 520 (2007).
20) J. Song, S. Kim, H. Sohn, T. Song, and Y. M. Yoo, Ultrasonics **50**, 613 (2010).
21) G. T. Clement, H. Nomura, and T. Kamakura, J. Acoust. Soc. Am. **130**, 1810 (2011).
22) T. Horino, T. Kamakura, H. Nomura, H. Adachi, and Y. Yasuno, Proc. 33rd Symp. Ultrasonic Electronics, 2012, p. 525 [in Japanese].
23) T. Kamakura, *Hisenkei Onkyogaku no Kiso* (Fundamentals of Nonlinear Acoustics) (Aichi Shuppan, Tokyo, 1996) Chap. 4 [in Japanese].
24) M. F. Hamilton, in *Nonlinear Acoustics*, ed. M. F. Hamilton and D. T. Blackstock (Academic Press, San Diego, CA, 1998) Chap. 8.
25) H. Nomura, H. Adachi, T. Kamakura, and G. T. Clement, Proc. Meet. Acoust. **19**, 045082 (2013).